

# Numerical Simulation of Incompressible Flows using Immersed Boundary Method Considering the Pressure Condition

Kyohei TAJIRI<sup>1</sup>, Hidetoshi NISHIDA<sup>1</sup> & Mitsuru TANAKA<sup>1</sup>

<sup>1</sup> Department of Mechanophysics, Kyoto Institute of Technology, Kyoto, Japan

Corresponding author: tajiri@kit.ac.jp

**Abstract:** In the Cartesian grid approach, the immersed boundary method (IBM) is well used to handle the flow around an object with a complicated shape. In this paper, in order to remove the unphysical pressure oscillations that appear in the conventional IBM, a new IBM approach is proposed. In the conventional IBM with the direct forcing, the unphysical pressure oscillations appear near the virtual boundary because of the pressure jump between inside and outside of the virtual boundary. In the present IBM approach, the velocity and pressure values inside the virtual boundary are not used. Therefore, the pressure jump, i.e., the cause of the pressure oscillations, does not appear. In the present IBM approach, when the pressure gradient value near the virtual boundary is calculated, the virtual pressure value inside the virtual boundary is estimated by considering the pressure condition on the virtual boundary. The present IBM approach is verified by the flows around a 2D circular cylinder which is a basic shape with curvilinear boundary. Then, it is concluded that the present IBM approach is very effective to remove the pressure oscillations that appear in the conventional IBM.

*Keywords:* Computational Fluid Dynamics, Computational Method, Cartesian Grid Approach, Immersed Boundary Method, Pressure Boundary Condition, Incompressible Flow.

## 1 Introduction

In recent years, many numerical simulations for the flow around an object with a complicated shape on the Cartesian coordinates are performed. Conventionally, the boundary fitted coordinates are adopted for the flow around an object with complicated shape. However, the boundary fitted coordinates require grid generation according to the object shape. As a result, the grid generation may consume a huge time for more complicated shapes. On the other hand, in the Cartesian coordinates, it is not necessary to newly generate the computational grid, even if the object with various shapes is included in the computational domain. Therefore, the Cartesian coordinates are efficient to simulate the flow around an object with complicated shape.

In the Cartesian grid approach, the immersed boundary method (IBM)[1] is well used to handle the flow around an object with a complicated shape. In the IBM, the boundary of the object is considered to be a cluster of virtual boundary point. In order to satisfy the velocity condition on the virtual boundary, e.g., the non-slip condition, the IBM requires only the additional forcing term in the momentum equations. Therefore, it is easy to apply the IBM to the object with complicated shape. In the estimation of the forcing term, the direct forcing[2] is generally adopted. However, the conventional IBM with the direct forcing generates the unphysical pressure oscillations near the virtual boundary because of the pressure jump between inside and outside of the virtual boundary. In order to remove the unphysical pressure oscillations, the seamless IBM

(SIBM)[3] was proposed. In the SIBM, the forcing term is added not only on the grid points near the virtual boundary but also in the region inside the virtual boundary. So far, many numerical simulations using the SIBM were performed successfully[4, 5]. In addition, the SIBM was also applied to the flow around a moving and deformable object[6]. However, in this simulation, only forced deformation of the object is considered. If the object is deformed by receiving force from the surrounding fluid, the exact prediction of the velocity condition inside the virtual boundary, which is necessary to estimate the forcing term, is difficult. In this paper, in order to remove the unphysical pressure oscillations, a new IBM approach which is not necessary to use the values (velocity and pressure) inside the virtual boundary is proposed. Therefore, the pressure jump i.e., the cause of the pressure oscillations, does not appear. In the present IBM approach, when the pressure gradient values near the virtual boundary is calculated, the virtual pressure values inside the virtual boundary is estimated by considering the pressure condition on the virtual boundary. Ikeno et al.[7] and Sato et al.[8] estimated the pressure gradient values near the virtual boundary by using interpolation of the pressure gradient values on the virtual boundary. However, in these papers, the pressure condition on the virtual boundary is simplified. In the estimation of the pressure gradient on the virtual boundary, the component values in the coordinate axis direction which there is the virtual boundary are assumed to be zero. For example, if there is the virtual boundary in the  $x$  direction, the pressure gradient on the virtual boundary is estimated to  $\frac{\partial p}{\partial x} = 0$ . In this paper, the pressure gradient in the normal direction on the virtual boundary is considered to be zero ( $\frac{\partial p}{\partial n} = 0$ ;  $n$  denotes the normal direction at the virtual boundary). In the present IBM approach, the pressure gradient values near the virtual boundary are estimated by using the virtual pressure values considering the pressure condition on the virtual boundary. Nishida[9] estimated the temperature values satisfying the temperature condition on the virtual boundary by using the Taylor series expansion. In the present IBM approach, the pressure values on the virtual boundary are estimated in reference to the method of Nishida. In this paper, it is discussed the removal property of the pressure oscillations in the present IBM approach.

## 2 Immersed Boundary Method

### 2.1 Governing equations

The non-dimensional continuity equation and incompressible Navier-Stokes equations are written as,

$$\frac{\partial u_i}{\partial x_i} = 0, \quad (1)$$

$$\frac{\partial u_i}{\partial t} = F_i - \frac{\partial p}{\partial x_i} + G_i, \quad (2)$$

where,  $Re$  denotes the Reynolds number defined by  $Re = L_0 U_0 / \nu_0$ .  $U_0$ ,  $L_0$  and  $\nu_0$  are the reference velocity, the reference length and the kinematic viscosity, respectively.  $u_i = (u, v)$  and  $p$  are the velocity components and the pressure.  $G_i$  in the momentum equations denotes the additional forcing term for the IBM.  $F_i$  denotes the convective and diffusion terms.

$$F_i = -u_j \frac{\partial u_i}{\partial x_j} + \frac{1}{Re} \frac{\partial^2 u_i}{\partial x_j \partial x_j}. \quad (3)$$

### 2.2 Numerical method

The incompressible Navier-Stokes equations (2) are solved by the second order finite difference method on the collocated grid arrangement. The convective, diffusion and pressure terms are discretized by the conventional second order centered finite difference method. For the time integration, the fractional step approach [10] based on the forward Euler method is applied. For the incompressible Navier-Stokes equations in the IBM, the fractional step approach can be written by

$$u_i^* = u_i^n + \Delta t F_i^n, \quad (4)$$

$$u_i^{n+1} = u_i^* + \Delta t \left( -\frac{\partial p^n}{\partial x_i} + G_i^n \right), \quad (5)$$

where  $u_i^*$  denotes the fractional step velocity and  $\Delta t$  is the time increment. The resulting pressure equation is solved by the BiCGSTAB method. In this paper, the convergence criterion of the pressure equation is  $1.0 \times 10^{-6}$ . Also, when the number of iterations is over 8000 times, the convergence criterion is  $1.0 \times 10^{-5}$ . Then, the conservation of mass is satisfied in the range of convergence criterion of the pressure equation.

### 2.3 Forcing term estimation

In order to adopt the IBM, the additional forcing term in the momentum equations,  $G_i$ , should be estimated. There are mainly two ways, that is, the feedback[11, 12] and direct[2] forcing term estimations. In this paper, the direct forcing term estimation is adopted.

The direct forcing term estimation is shown in Fig. 1. In the figure,  $I, J$  are the grid index. The forcing term can be determined by

$$G_i^n = -F_i^n + \frac{\partial p^n}{\partial x_i} + \frac{\bar{U}_i^{n+1} - u_i^n}{\Delta t}, \quad (6)$$

where  $\bar{U}_i^{n+1}$  denotes the linearly interpolated velocity. Namely, the forcing term is specified as the velocity components at next time step satisfy the relation,  $u_i^{n+1} = \bar{U}_i^{n+1}$ . In the forcing term estimation for the IBM, the grid points added forcing term are restricted near the virtual boundary only. In this approach, the non-negligible velocity appears inside the virtual boundary. Also, the pressure distributions near the virtual boundary show the unphysical oscillations because of the pressure jump. In the present IBM approach, the governing equations are solved only outside the virtual boundary by considering the pressure condition on the virtual boundary in order to avoid the pressure jump.

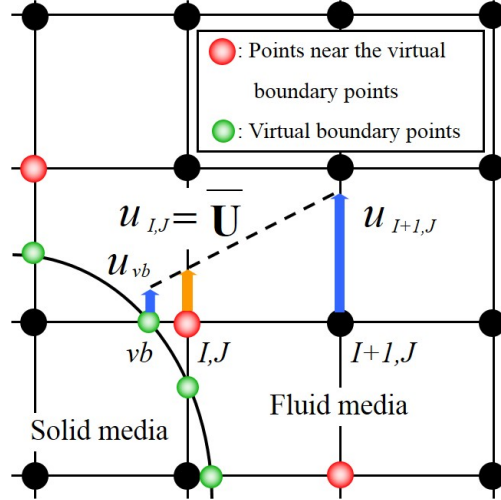


Figure 1: Grid points added forcing terms.

### 2.4 Differential expression near the virtual boundary

For the pressure, the pressure condition on the virtual boundary ( $\frac{\partial p}{\partial n} = 0$ ) is considered. The pressure value on the virtual boundary is estimated by using the Taylor series expansion. For example, in Fig. 2, the pressure value on the virtual boundary point,  $vb$ , is estimated by using the Taylor series expansion in two variables with reference to the points  $m = 1$  to 3. In Fig. 2,  $\mathbf{n} = (n_x, n_y)$  denotes the unit normal vector at the virtual boundary point. The reference points are chosen from the surrounding grid points in the normal direction. The relationship between pressure on the virtual boundary and reference points is approximated

by

$$p_m = p_{vb} + \left( l_{mx} \frac{\partial p}{\partial x} \Big|_{vb} + l_{my} \frac{\partial p}{\partial y} \Big|_{vb} \right) + \frac{1}{2} \left( l_{mx}^2 \frac{\partial^2 p}{\partial x^2} \Big|_{vb} + 2l_{mx}l_{my} \frac{\partial^2 p}{\partial x \partial y} \Big|_{vb} + l_{my}^2 \frac{\partial^2 p}{\partial y^2} \Big|_{vb} \right), \quad (7)$$

where  $l_{mx}$ ,  $l_{my}$  are the distance components from the virtual boundary point to the reference points. The pressure condition on the virtual boundary is written by

$$\frac{\partial p}{\partial n} \Big|_{vb} = n_x \frac{\partial p}{\partial x} \Big|_{vb} + n_y \frac{\partial p}{\partial y} \Big|_{vb} = 0. \quad (8)$$

By substituting the equation (8), the equation (7) is rewritten to

$$p_m = p_{vb} + \left( l_{mx} - \frac{n_x l_{my}}{n_y} \right) \frac{\partial p}{\partial x} \Big|_{vb} + \frac{1}{2} \left( l_{mx}^2 - 2 \frac{n_x l_{mx} l_{my}}{n_y} + \frac{n_x^2 l_{my}^2}{n_y^2} \right) \frac{\partial^2 p}{\partial x^2} \Big|_{vb}. \quad (9)$$

Then, the pressure value on the virtual boundary  $p_{vb}$  can be determined by

$$p_{vb} = \frac{1}{C} [(A_2 B_3 - A_3 B_2) p_1 + (A_3 B_1 - A_1 B_3) p_2 + (A_1 B_2 - A_2 B_1) p_3], \quad (10)$$

$$A_m = l_{mx} - \frac{n_x l_{my}}{n_y}, \quad (11)$$

$$B_m = \frac{1}{2} \left( l_{mx}^2 - 2 \frac{n_x l_{mx} l_{my}}{n_y} + \frac{n_x^2 l_{my}^2}{n_y^2} \right), \quad (12)$$

$$C = A_1(B_2 - B_3) + A_2(B_3 - B_1) + A_3(B_1 - B_2). \quad (13)$$

The pressure value on the grid point  $(I-1, J)$  is calculated by

$$p_{I-1,J} = \frac{(|l_{m1}| - \Delta x) p_{vb} + \Delta x p_{I,J}}{|l_{m1}|}, \quad (14)$$

where,  $\Delta x$  is the grid spacing in the  $x$  direction. As a result, discretization on the grid point  $(I, J)$  is handled in the same manner as other grid points by using the calculated pressure value  $p_{I-1,J}$ . In this study, the pressure equation is solved by fixing the pressure value obtained by the above procedure.

For the velocity, the velocity gradient on the grid point  $(I, J)$  near the virtual boundary is represented by one-sided difference written in

$$\frac{\partial u}{\partial x} \Big|_{I,J} = \frac{-3u_{I,J} + 4u_{I+1,J} - u_{I+2,J}}{2\Delta x}. \quad (15)$$

### 3 Flow around a 2D stationary circular cylinder

In order to validate the present IBM approach, the flow around a 2D stationary circular cylinder is considered. The computational domain is shown in Fig. 3. Diameter of the circular cylinder is  $D = 1$  and  $\theta$  is an angle from rear stagnation point of the circular cylinder. The computational grid is the hierarchical Cartesian grid. In this paper, the simulation is performed on three grids to investigate the influence of the grid resolution. The grid resolutions near the virtual boundary are  $\Delta = \Delta x = \Delta y = 0.025, 0.0125$  and  $0.00625$  respectively. The time increment is  $\Delta t = 0.001, 0.0005$  and  $0.00025$  in each simulation. The impulsive start determined by the uniform flow ( $u = 1, v = 0$ ) is adopted. On the inflow boundary, the velocity is fixed by the uniform flow and the pressure is imposed by the Neumann condition obtained by the normal momentum equation. The velocity is extrapolated from the inner points and the pressure is obtained by the Sommerfeld radiation condition[13] on the outflow and side boundaries. On the virtual boundary, the velocity condition is the non-slip ( $u = 0, v = 0$ ) condition. The Reynolds number is set as  $Re = 40$  and  $200$ .

Figure 4 shows the pressure coefficient  $C_p$  distributions at each grid resolution in  $Re = 40$ . The pressure

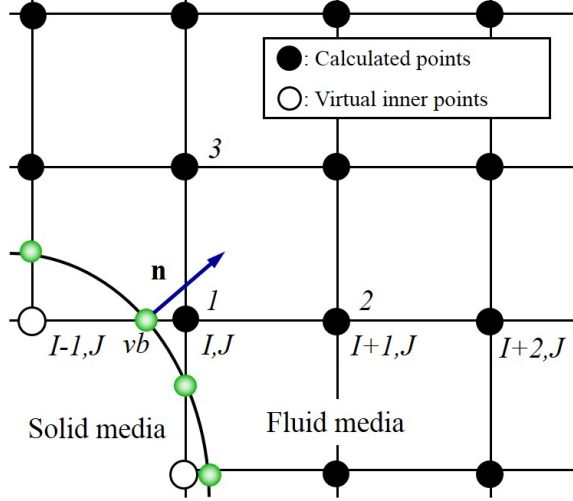


Figure 2: Handling near the virtual boundary.

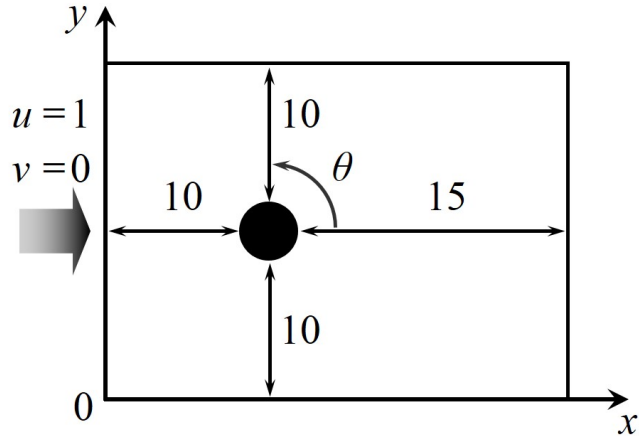


Figure 3: Computational domain for 2D stationary circular cylinder.

values on the virtual boundary is interpolated from the grid points around the virtual boundary. At  $\Delta = 0.025$ , the oscillations of the pressure coefficient appear because of coarse resolution. On the other hand, at  $\Delta = 0.0125$  and  $0.00625$ , the pressure oscillations do not appear and the pressure coefficients are in good agreement with each other. In Table 1, the drag coefficient, the wake length and the pressure difference between front and rear stagnation points are shown with the reference results[14, 15]. In this paper, the drag coefficient is estimated by

$$C_D = \frac{\int_b p_x ds + \int_b \tau_x ds}{\frac{1}{2} \rho_0 U_0^2 S}, \quad (16)$$

where  $b$  denotes the virtual boundary,  $p_x$  and  $\tau_x$  denote the  $x$  direction components of the interpolated pressure and shear stress on the circular cylinder surface.  $\rho_0$  and  $U_0$  denote the reference density and velocity of the flow. In particular, the results at  $\Delta = 0.0125$  and  $0.00625$  are in good agreement with each other. Furthermore, it is found that the present IBM results are in good agreement with the reference ones. Figure 5 shows the pressure contours at  $\Delta = 0.0125$ . Near the virtual boundary, the pressure oscillations do not appear, and the smooth pressure distribution is obtained. Also, it is speculated that the pressure

condition on the virtual boundary is satisfied from the pressure distribution near the virtual boundary.

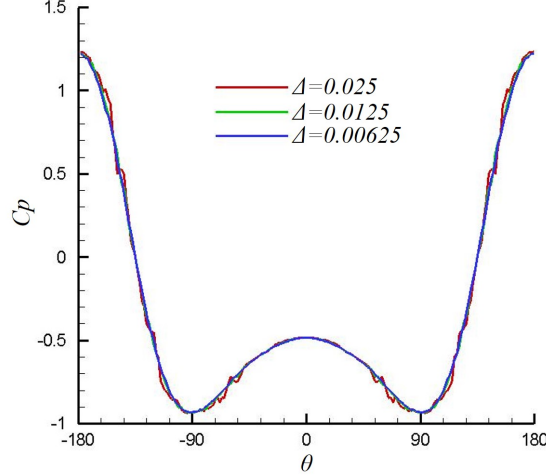


Figure 4: Pressure coefficient distributions for 2D stationary circular cylinder ( $Re = 40$ ).

Table 1: Comparison of characteristic quantities for 2D stationary circular cylinder ( $Re = 40$ ).

	$C_D$	$L_V/D$	$PE$
$\Delta = 0.025$	1.517	2.300	0.858
$\Delta = 0.0125$	1.541	2.310	0.854
$\Delta = 0.00625$	1.553	2.310	0.854
Nishida et al.[3] (SIBM)	1.501	2.336	0.847
Dennis et al.[14]	1.522	2.345	0.826
Fornberg[15]	1.498	2.240	0.800

Figure 6 shows the pressure coefficient distributions on each grid in  $Re = 200$  at the time which the lift coefficient is maximum. At  $\Delta = 0.025$ , the pressure oscillations appear. However, at  $\Delta = 0.0125$  and  $0.0625$ , the pressure oscillations do not appear and the pressure coefficients are in good agreement with each other. In Table 2, the time-averaged drag coefficient, the amplitude of lift coefficient and the Strouhal number are shown with the reference results[3, 16]. The lift coefficient is estimated by

$$C_L = \frac{\int_b p_y ds + \int_b \tau_y ds}{\frac{1}{2} \rho_0 U_0^2 S}, \quad (17)$$

where  $p_y$  and  $\tau_y$  denote the  $y$  direction components of the interpolated pressure and shear stress on the circular cylinder surface. It is found that the present IBM results are in good agreement with the reference ones. Figure 7 shows the pressure contours at  $\Delta = 0.0125$ . In the unsteady flow field, very smooth pressure distribution is obtained. Then, it can be found that the present IBM approach is effective to remove the pressure oscillations that appear in the conventional IBM.

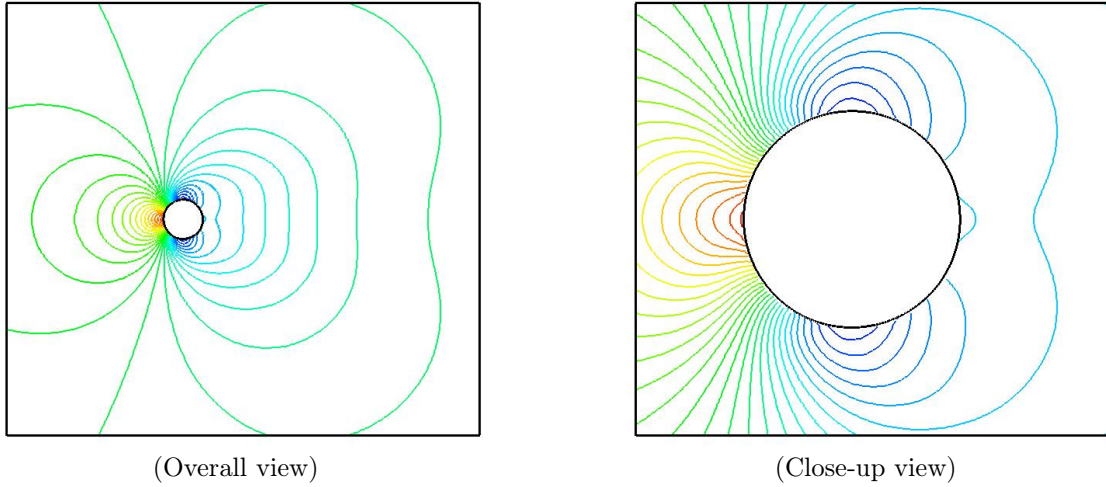


Figure 5: Pressure contours for 2D stationary at  $\Delta = 0.0125$  ( $Re = 40$ ).

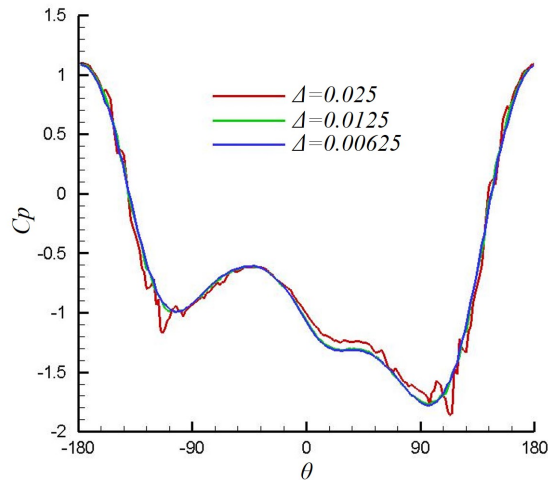


Figure 6: Pressure coefficient distributions for 2D stationary circular cylinder ( $Re = 200$ ).

Table 2: Comparison of characteristic quantities for 2D stationary circular cylinder ( $Re = 200$ ).

	$\bar{C}_D$	$C_{L_{amp}}$	$St$
$\Delta = 0.025$	1.257	0.615	0.200
$\Delta = 0.0125$	1.349	0.682	0.199
$\Delta = 0.00625$	1.359	0.697	0.199
Nishida et al.[3] (SIBM)	1.316	0.677	0.200
Rosenfeld[16]	1.329	0.674	0.197

## 4 Flow around a 2D oscillating circular cylinder

In order to validate the present IBM approach for the moving boundary problem, the flow around a 2D oscillating circular cylinder is considered. The computational domain is shown in Fig. 8. The circular

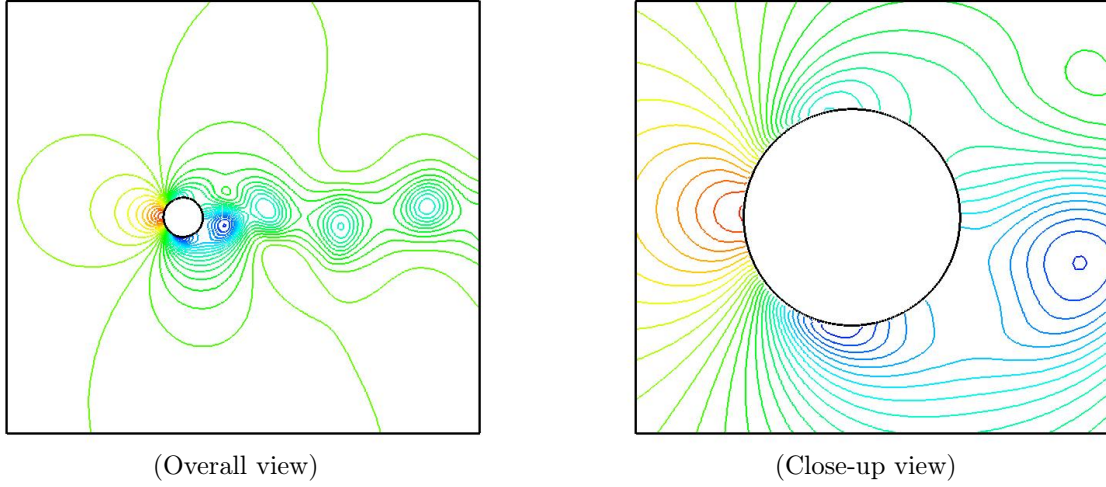


Figure 7: Pressure contours for 2D stationary circular cylinder at  $\Delta = 0.0125$  ( $Re = 200$ ).

cylinder in the uniform flow moves vertically as,

$$x(t) = x_0, \quad (18)$$

$$y(t) = y_0 + \frac{y_{amp}}{2} \sin(2\pi ft), \quad (19)$$

where  $x(t)$ ,  $y(t)$  are location of the circular cylinder at non-dimensional time  $t$ . The initial location of the circular cylinder is  $(x_0, y_0) = (10.5, 10.5)$ .  $y_{amp}/2$ ,  $f$  denote the amplitude and the frequency. In this paper, these are set as  $y_{amp}/2 = 0.2$  and  $f = 0.2$ . The computational grid is the hierarchical Cartesian grid. The grid resolution is set as  $\Delta = 0.0125$  at near the circular cylinder from the results of simulation of the flow around a stationary circular cylinder. The time increment is set as  $\Delta t = 0.001$ . The initial and boundary conditions are the same as the previous simulation. On the virtual boundary, the velocity of the moving circular cylinder ( $u = 0$ ,  $v = \frac{dy}{dt}$ ) is considered. The Reynolds number is set as  $Re = 200$ .

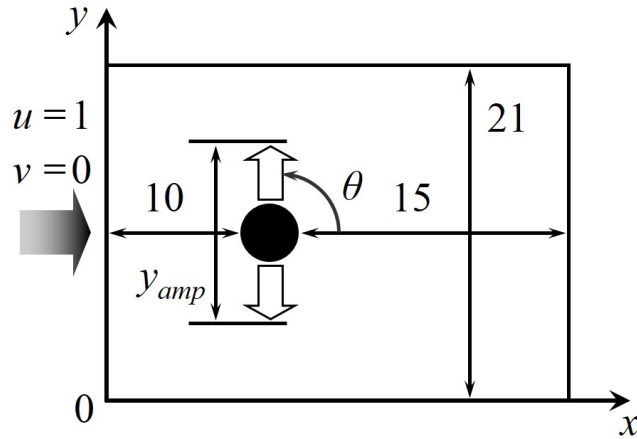


Figure 8: Computational domain for 2D oscillating circular cylinder.

Figure 9 shows the pressure contours at  $t = 113.75$  and  $115$ . At  $t = 113.75$ , the circular cylinder is located at the bottom dead center ( $y = 10.3$ ). At  $t = 115$ , the circular cylinder is located at the initial

position ( $y = 10.5$ ) and is moving upward. Figure 10 shows the pressure coefficient distribution in  $Re = 200$  at  $t = 115$ . In Fig. 9, it can be observed that smooth pressure distribution is obtained. In Fig. 10, the oscillations of the pressure coefficient appear but the scale is very small.

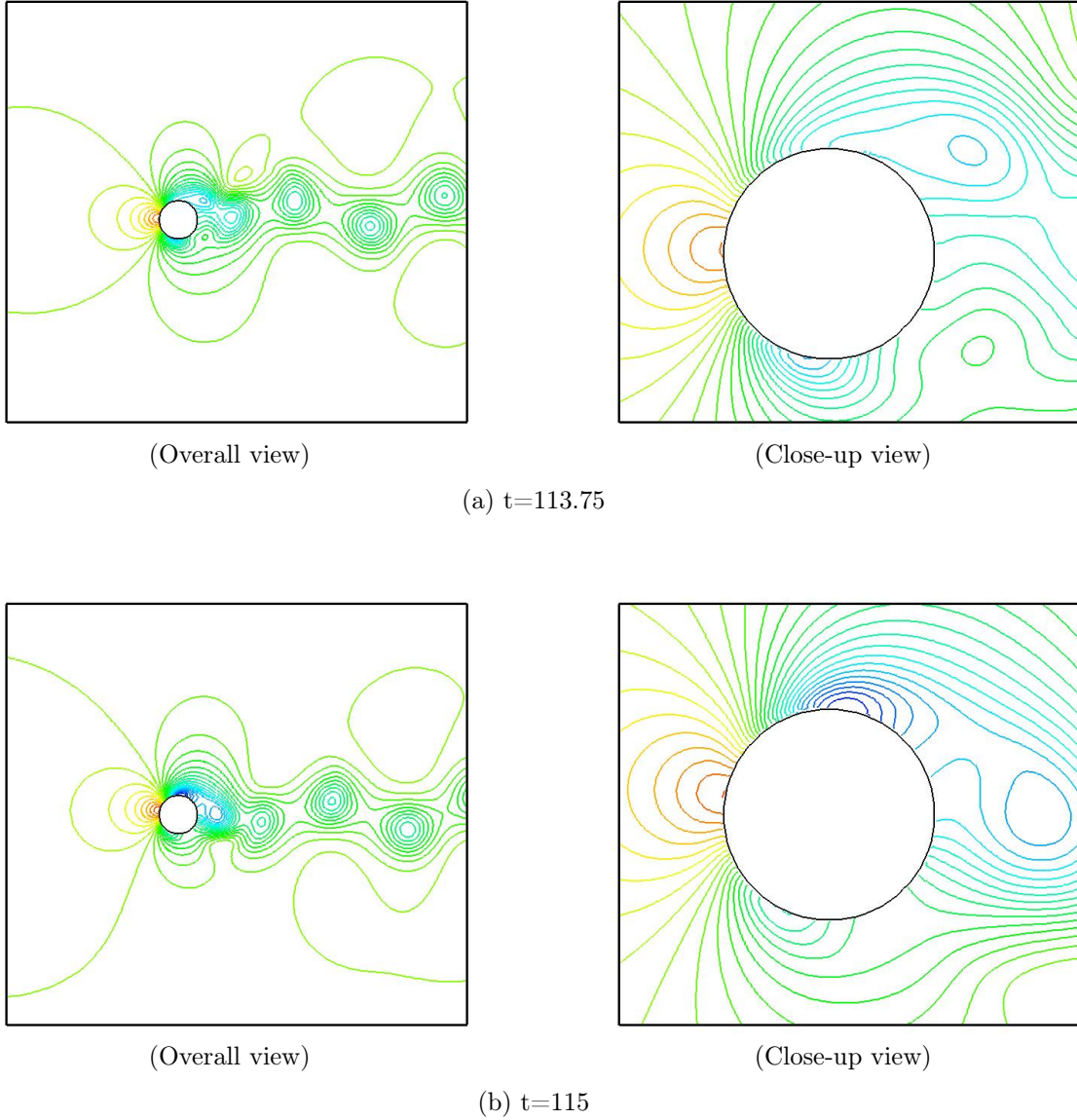


Figure 9: Pressure contours for 2D oscillating circular cylinder at  $\Delta = 0.0125$  ( $Re = 200$ ).

In Fig. 11, the time history of the drag and lift coefficients are shown. In Table 3, the time-averaged drag and lift coefficients and the Strouhal number are shown with the reference results[17]. The time-averaged drag coefficient is in good agreement with the reference result. However, the non-negligible oscillations of the drag and lift coefficients appear in Fig. 11. This is because the forcing points change by moving the virtual boundary. As a result, the amplitude of the lift coefficient in Table 3 is larger than the reference result.

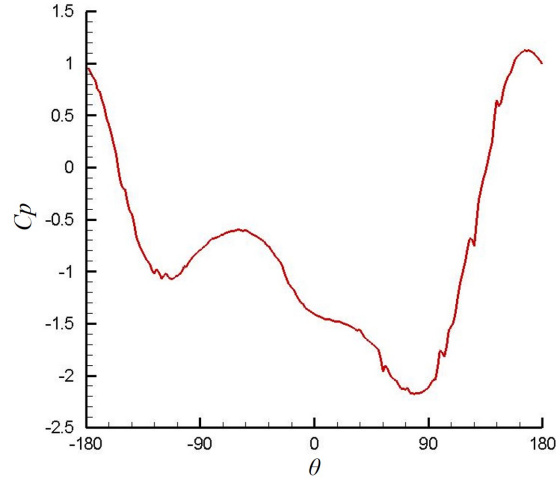


Figure 10: Pressure coefficient distribution for 2D oscillating circular cylinder ( $Re = 200$ ).

Table 3: Comparison of characteristic quantities for 2D oscillating circular cylinder ( $Re = 200$ ).

	$\bar{C}_D$	$C_L$	$St$
Present	1.55	$\pm 0.76$	0.20
Wu et al.[17]	1.58	$\pm 0.58$	0.20

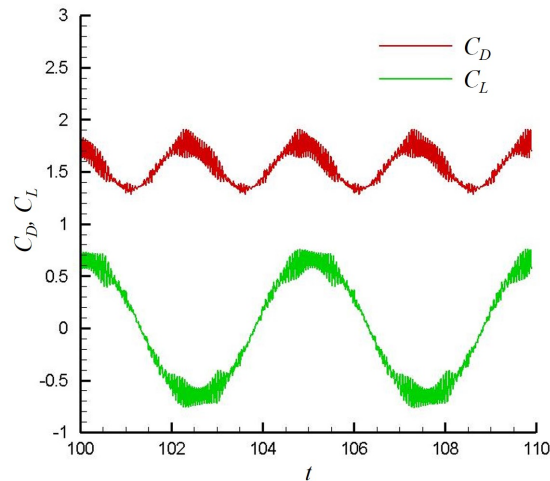


Figure 11: Time history of drag and lift coefficients for 2D oscillating circular cylinder ( $Re = 200$ ).

## 5 Concluding Remarks

In this paper, in order to remove the unphysical pressure oscillations, a new IBM approach which is not necessary to use the values (velocity and pressure) inside the virtual boundary was proposed. In the present IBM approach, when the pressure gradient value near the virtual boundary is calculated, the virtual pressure value inside the virtual boundary is estimated by considering the pressure condition on the virtual boundary. In order to validate the present IBM approach, the numerical simulations of incompressible flow around a

2D circular cylinder which is a basic shape with curvilinear boundary were considered. Firstly, the present IBM approach was applied to a 2D stationary circular cylinder at some grid resolutions ( $\Delta = 0.025, 0.0125$  and  $0.00625$ ). At  $\Delta = 0.025$ , the oscillations of the pressure coefficient appear. On the other hand, at  $\Delta = 0.0125$  and  $0.00625$ , the pressure oscillations did not appear and the pressure coefficients were in good agreement with each other. Furthermore, these results were in good agreement with the reference ones. Then, it is concluded that the present IBM approach is very effective to remove the pressure oscillations that appear in the conventional IBM. Secondly, the present IBM approach was applied to the flow around a 2D oscillating circular cylinder. The resulting time-averaged drag coefficient was in good agreement with reference result. However, the oscillations of the resulting coefficients associated with time appeared. This is because the forcing points change by moving the virtual boundary. Therefore, in the case of applying the present IBM approach to the moving boundary problem, it is necessary to consider the treatment to reduce the oscillations.

## References

- [1] C. S. Peskin and D. M. McQueen. A three-dimensional computational method for blood flow in the heart I. immersed elastic fibers in a viscous incompressible fluid. *Journal of Computational Physics*, 81(2):372–405, 1989.
- [2] E. A. Fadlun, R. Verzicco, P. Orlandi, and J. Mohd-Yosof. Combined immersed-boundary finite-difference methods for three-dimensional complex simulations. *Journal of Computational Physics*, 161(1):35–60, 2000.
- [3] H. Nishida and K. Sasao. Incompressible Flow Simulations Using Virtual Boundary Method with New Direct Forcing Terms Estimation. *Proceedings of International Conference on Computational Fluid Dynamics 2006(Springer)*, pages 185–186, 2006.
- [4] H. Nishida and K. Tajiri. Numerical simulation of incompressible flows around a fish model at low Reynolds number using seamless virtual boundary method. *Journal of Fluid Science and Technology*, 4(3):500–511, 2009.
- [5] K. Tajiri, H. Nishida, and M. Tanaka. Property of Seamless Immersed Boundary Method for Large Eddy Simulation of Incompressible Turbulent Flows. *Journal of Fluid Science and Technology*, 9(2):1–8, 2014.
- [6] K. Tajiri, H. Nishida, and M. Tanaka. Property of Seamless Immersed Boundary Method for Large Eddy Simulation of Incompressible Turbulent Flows. *Proceedings of 8th International Conference on Computational Fluid Dynamics*, (ICCFD8-2014-0197):1–13, 2014.
- [7] T. Ikeno and T. Kajishima. Finite-difference immersed boundary method consistent with wall conditions for incompressible turbulent flow simulations. *Journal of Computational Physics*, 226:1–15, 2007.
- [8] N. Sato, T. Kajishima, S. Takeuchi, M. Inagaki, and N. Horinouchi. A Direct Discretization Approach near Wall Boundaries for a Cartesian Grid Method(Consideration of Consistency between Velocity and Pressure Fields) (in Japanese). *Transactions of the Japan Society of Mechanical Engineers Series B*, 79(800):605–621, 2013.
- [9] H. Nishida. Development of Seamless Immersed Boundary Method to Various Partial Differential Equations. *Proceedings of Korea-Japan CFD Workshop 2015*, pages 1–15, 2015.
- [10] C. M. Rhie and W. L. Chow. Numerical Study of the Turbulent Flow Past an Airfoil with Trailing Edge Separation. *AIAA Journal*, 21(11):1525–1532, 1983.
- [11] D. Goldstein, R. Handler, and L. Sirovich. Modeling a no-slip flow boundary with an external force field. *Journal of Computational Physics*, 105(2):354–366, 1993.
- [12] E. M. Saiki and S. Biringen. Numerical simulation of a cylinder in uniform flow: application of a virtual boundary method. *Journal of Computational Physics*, 123(2):450–465, 1996.
- [13] K. Kawakami, H. Nishida, and N. Satofuka. An open boundary condition for the numerical analysis of unsteady incompressible flow using the vorticity-streamfunction formulation (in Japanese). *Transactions of the Japan Society of Mechanical Engineers Series B*, 60(574):1891–1896, 1994.
- [14] S. C. R. Dennis and G. Z. Chang. Numerical solutions for steady flow past a circular cylinder at Reynolds numbers up to 100. *Journal of Fluid Mechanics*, 42(3):471–489, 1970.

- [15] B. Fornberg. A numerical study of steady viscous flow past a circular cylinder. *Journal of Fluid Mechanics*, 98(4):819–855, 1980.
- [16] M. Rosenfeld. Grid refinement test of time-periodic flows over bluff bodies. *Computers & Fluids*, 23(5):693–709, 1994.
- [17] G. Wu, B. Piao, and S. Kuroda. Development of Cut Cell Method for Incompressible Fluid Flows with Moving Boundary. *Proceedings of Mechanical Engineering Congress, 2005 Japan*, 2005(2):111–112, 2005. (Japanese).